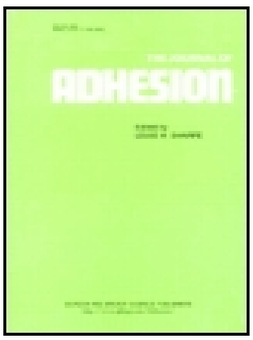

The Journal of Adhesion

ISSN: 0021-8464 (Print) 1545-5823 (Online) Journal homepage: http://www.tandfonline.com/loi/gadh20

Adhesion of a rigid punch to a confined elastic layer revisited

René Hensel, Robert M. McMeeking & Attila Kossa

To cite this article: René Hensel, Robert M. McMeeking & Attila Kossa (2017): Adhesion of a rigid punch to a confined elastic layer revisited, The Journal of Adhesion, DOI: 10.1080/00218464.2017.1381603

To link to this article: https://doi.org/10.1080/00218464.2017.1381603

Accepted author version posted online: 28 Nov 2017.
Published online: 14 Feb 2018.

THE JOURNAL OF ADHESION
https://doi.org/10.1080/00218464.2017.1381603

Taylor & Francis
Taylor & Francis Group

Adhesion of a rigid punch to a confined elastic layer revisited

René Hensel [a,b], Robert M. McMeeking[a,b,c], and Attila Kossa[b,d]

[a]INM – Leibniz Institute for New Materials, Saarbrücken, Germany; [b]Materials and Mechanical Engineering Departments, University of California, Santa Barbara, CA, USA; [c]Engineering School, University of Aberdeen, King's College, Aberdeen, UK; [d]Department of Applied Mechanics, Budapest University of Technology and Economics, Budapest, Hungary

ABSTRACT

The adhesion of a punch to a linear elastic, confined layer is investigated. Numerical analysis is performed to determine the equivalent elastic modulus in terms of layer confinement. The size of the layer relative to the punch radius and its Poisson's ratio are found to affect the layer stiffness. The results reveal that the equivalent modulus of a highly confined layer depends on its Poisson's ratio, whereas, in contrast, an unconfined layer is only sensitive to the extent of the elastic film. The solutions of the equivalent modulus obtained from the simulations are fitted by an analytical function that, subsequently, is utilized to deduce the energy release rate for detachment of the punch via linear elastic fracture mechanics. The energy release rate strongly varies with layer confinement. Regimes for stable and unstable crack growth can be identified that, in turn, are correlated to interfacial stress distributions to distinguish between different detachment mechanisms.

ARTICLE HISTORY
Received 6 June 2017
Accepted 15 September 2017

KEYWORDS
Stress distribution; finite element analysis; dry adhesion; pressure-sensitive; tack

Introduction

Confined adhesive layers are commonly present in a great variety of technical applications and natural systems. Examples include pressure sensitive adhesives[1–4], adhesive hydrogel films[5–7], micropatterned adhesives[8,9], and the adhesive secretions of (fouling) species sticking to a diversity of substrates[10–12]. The adhesion and contact mechanics of such confined layers depends not only on material properties but also on the boundary conditions and the degree of confinement. To characterize this situation in the present paper, we consider a rigid punch adhering to a linear elastic layer immobilized on a rigid substrate, as illustrated in Figure 1. Because of its simple setup, such adhesion, in the form of the tack test, is widely used to probe adhesive characteristics.

Theoretical concepts describing the fundamental mechanics involved have been well known since the middle of the last century[11,13–16]. In general, the

CONTACT René Hensel rene.hensel@leibniz-inm.de INM – Leibniz Institute for New Materials, Campus D2.2, Saarbrücken 66123, Germany.

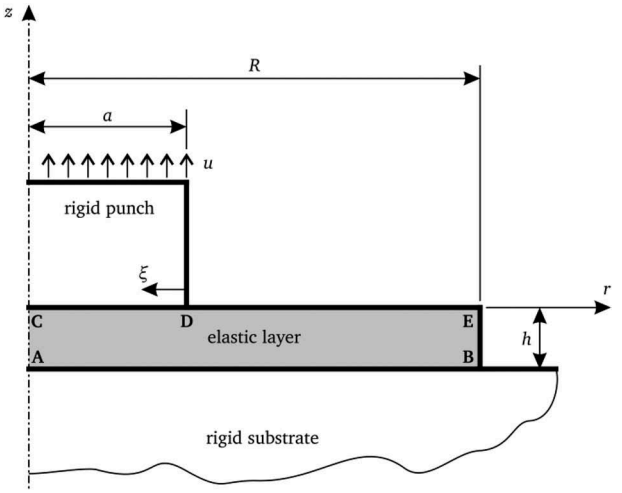

Figure 1. An axisymmetric cylindrical rigid punch adhering to a confined elastic layer immobilized on a rigid substrate.

detachment of two adhering surfaces is related to the adhesion energy, w, and the energy release rate, G, given by

$$G = \frac{\partial U}{\partial A}, \tag{1}$$

where U is the system potential energy and A is the area of contact that is diminished by an increment of detachment. Based on such a fracture mechanics approach as first introduced by Griffith[17], Kendall considered two limiting cases for an elastic, incompressible film (*i.e.* with Poisson's ratio $\upsilon = 0.5$) sandwiched between a rigid punch and a rigid substrate[13]: (i) the elastic layer is very thick compared to the radius, a, of the punch *i.e.* $h \gg a$, where h is the thickness of the layer; and (ii) the layer is very thin compared to the punch radius. For case (i) Kendall obtained the following equation for the pull-off stress:

$$\sigma_p = \sqrt{\frac{32EG}{3\pi a}}, \tag{2}$$

where σ_p is defined as the force to detach the punch divided by the cross-sectional area of the punch, and E is Young's modulus of the layer. Thus, σ_p scales with the punch radius $a^{-0.5}$. For case (ii), that is $h \ll a$, the pull-off stress is[11]:

$$\sigma_p = \sqrt{\frac{2EG}{h}}. \tag{3}$$

Here, the pull-off stress scales with the layer thickness $h^{-0.5}$ and, in contrast to case (i), is insensitive to the punch radius. However, configurations of interest rarely conform to the limiting cases, *e.g.* elastic films with thicknesses

similar to the punch radius. This intermediate case ($h \approx a$) must be considered independently.

Ganghoffer and Gent[16] first treated this problem based on a finite element analysis for linearly elastic materials by calculating the equivalent modulus, $\bar{E}$, in terms of the confinement, a/h, as follows:

$$\bar{E} = \frac{\bar{\sigma}}{\bar{\varepsilon}} = \frac{F/A}{u/h} = \frac{2Uh}{u^2 a^2 \pi}, \tag{4}$$

where $\bar{\sigma}$ is the average axial stress in the layer over the contact area, $\bar{\varepsilon}$ is the effective axial strain in the layer, F is the load applied to the punch, u is the punch displacement (see Figure 1), and U is the strain energy stored in the layer. In displacement control, U is thus the potential energy of the system. Based on Ganghoffer's and Gent's numerical data, a semi-empirical analytical function for the compliance, C, of the elastic layer as a function of a/h was derived by Shull et al.[1]. Nowadays, their function is widely used for analyzing experimental results. For example, the compliance can be easily inserted into Equation. (1) to deduce the energy release rate, in turn determining adhesion performance. One can then distinguish between stable and unstable regimes of crack growth[2,3,18]. However, there are indications that the analytical function for compliance overestimates experimental data in some cases[3]. Thus it is desirable to revisit the stress analysis of the tack test to provide more accurate estimates of compliances and energy release rates.

Furthermore, the interfacial stress distribution at the interface between the rigid probe and the adhesive elastic layer is of particular importance for gaining insights regarding different detachment mechanisms. Experimental work indicates that for circular punches there exists a transition from axisymmetric edge crack detachment to edge cracks exhibiting fingering instabilities[19–21]. Sometimes interfacial cavitation occurs with increasing confinement of the layer[21–23]. These phenomena provide additional motivation for undertaking further stress analysis of the tack test.

Although the experimental configuration illustrated in Figure 1 has frequently been used and analyzed in the past, there remain challenges and open questions that are addressed in the present paper: First, the mesh size used for numerical simulations and its impact on the equivalent modulus is investigated and the outcomes compared to Ganghoffer's and Gent's[16] results. An improved mesh design addressing the presence of a corner stress singularity is introduced. Second, the equivalent modulus, $\bar{E}$, as a function of the confinement (h/a), Poisson's ratio (ν), and the radius of the film (R) is computed, thereby providing detailed insights into the influence of geometric parameters and material properties of the elastic layer in a manner that augments those already in the literature. Third, we propose a new analytical function for $\bar{E}$ based on the numerical values obtained, that, being based on our new, more accurate results, is a more reliable characterization of the effective elasticity of the confined elastic

layer than has been provided previously. The semi-empirical function is then used to calculate the energy release rate, and therefore to provide a better estimate of the driving force for detachment of a stiff punch from the confined elastic layer to which it is adhered. Finally, the interfacial stress distribution at the punch is computed and, in correlation to the energy release rate, these results are utilized to classify detachment mechanisms.

Finite element model

Figure 1 illustrates the axisymmetric problem treated in the present paper: A rigid cylindrical punch adheres to an elastic layer that is immobilized on a rigid substrate. The elastic layer at the interface **AB** is fixed ($u_r = u_\theta = u_z = 0$), whereas a vertical displacement ($u_z = u$) is imposed on it along the interface **CD**, but without horizontal displacement (no slip condition). It should be noted that in such conditions a displacement applied to the punch becomes a prescribed displacement on the punch-layer interface **CD**, because of the rigidity of the punch. It should be further noted that stress singularities are expected at the locations B and D. The coordinates r, θ, and z represent the radial, circumferential and axial directions. The thickness of the elastic layer is h, the radius of the punch is a, and the outer radius of the circular elastic layer is R. The Young's modulus of the layer is set to $E = 1$ MPa, whereas the Poisson's ratio is varied from 0.48 to 0.4999999. The finite element simulations are obtained using the commercial finite element software ABAQUS 2016 (SIMULIA, Maastricht, Netherlands). Eight-node axisymmetric elements (CAX8) are used with full numerical integration for Poisson's ratios ≤ 0.495. For Poisson's ratios > 0.495, hybrid elements (CAX8H) are employed. It should be noted that the results presented in the present paper are based on linear elastic fracture mechanics, whereas viscoelasticity and large deformations are not accounted for.

Numerical results

Comparison of mesh designs

First, we compare results from three different finite element mesh configurations (as illustrated in Figure 2) to investigate the effect of mesh design and element density on the equivalent modulus. The 3 configurations are:

(i) The mesh used by Ganghoffer and Gent[16], (Figure 2a),
(ii) A uniform mesh of square elements. The size of the elements is a/n, where n varies from 1 to 512 (Figure 2b),
(iii) A mesh having focused arrangements at the corner singularity locations B and D (Figure 2c, d). The smallest element size was 10^{-4}, whereas the maximum element size was min $(1/25, h/25)$. The

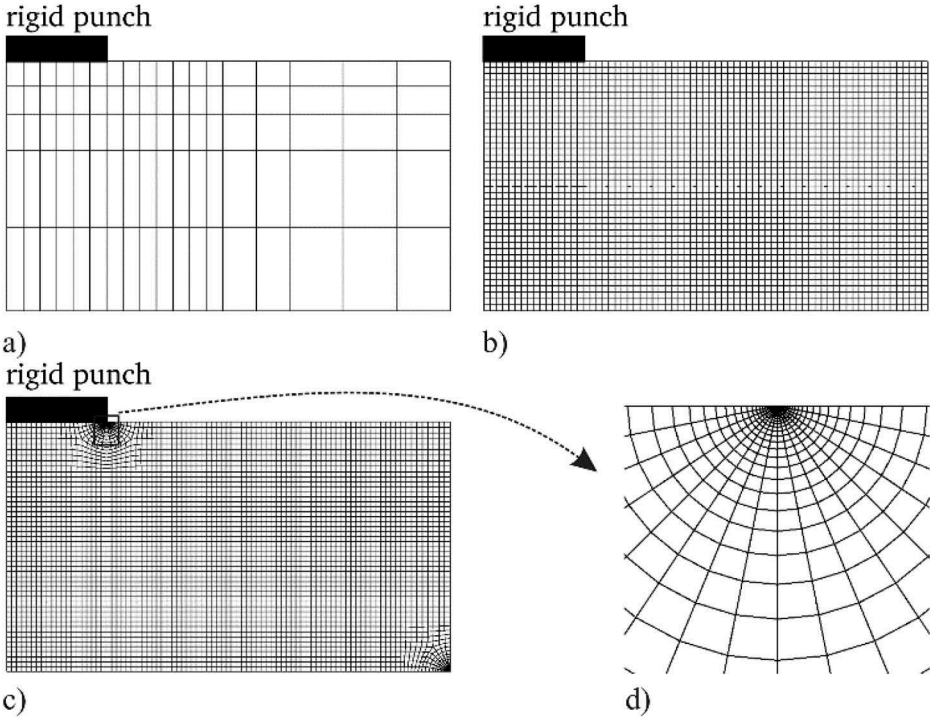

Figure 2. Representative mesh designs used in the present study. (**a**) The mesh used by Ganghoffer and Gent[16]. (**b**) A mesh of uniform square elements of element size a/n, where a is the punch radius and n is an integer that varies from 1 to 512. (**c**) The mesh having focused arrangements at the corner singularities. (**d**) Magnified region of the focused mesh at the corner of the punch.

transition from the minimum to the maximum element size is limited to the region min $(h/2, 0.1)$.

For the comparison of the different mesh strategies the following conditions are chosen (adopted from ref[16]): the elastic layer has $h/a = 2.5$, the configuration of the elastic layer is $R/a = 16/9 = 4.4444$, and Poisson's ratio is $\nu = 0.495$. The results for the equivalent modulus, normalized by Young's modulus, E, are illustrated in Figure 3 and summarized in Table 1. It can be seen clearly that the results vary with mesh design. Specifically, the meshes composed of quadrilateral elements of uniform size reveal that, as expected, a higher number of elements (*i.e.* a finer mesh) leads to a smaller value of the equivalent modulus. As the mesh is refined, the values obtained should tend toward an asymptotic value, the unknown exact solution (to within residual numerical error). Based on this insight, the exact value for the equivalent modulus is most probably slightly less than the value corresponding to the result from the mesh having $n = 512$.

The equivalent modulus obtained with the mesh design having focused arrangements at the locations of stress singularities is slightly smaller compared to that computed using the finest mesh of uniform quadrilateral elements with

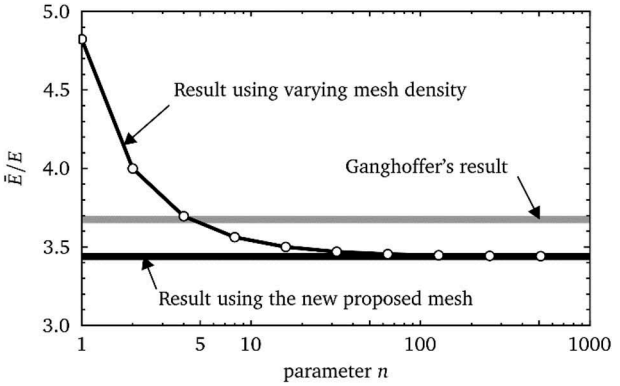

Figure 3. The equivalent modulus computed from the various mesh designs (see Figure 2). The elastic layer has the following dimensions: $h/a = 2.5$, $R/a = 16/9$. Poisson's ratio is $\nu = 0.495$. The result highlighted as Ganghoffer's is from ref.[16].

Table 1. Normalized equivalent moduli, $\bar{E}/E$, obtained using the various meshes (see Figures 2 and 3).

	n	Number of elements	Number of nodes	$\bar{E}/E$
i) Mesh from ref.[16]		90	317	3.6752
ii) Mesh of square elements with element size a/n	1	12	51	4.8237
	2	45	164	3.9994
	4	180	597	3.6958
	8	720	2273	3.5622
	16	2840	8743	3.4999
	32	11360	34525	3.4694
	64	45440	137209	3.4543
	128	182080	548019	3.4469
	256	728320	2188517	3.4432
	512	2913280	8746953	3.4413
iii) Mesh with focused arrangements at B and D.		5105	25930	3.4396

$n = 512$. We conclude that this mesh design most likely provides the most accurate values for the equivalent modulus among all the mesh designs considered in our study. We emphasize that the equivalent modulus obtained using Ganghoffer's and Gent's[16] mesh design is in error by 6.85% compared to the best result from the improved mesh designs. Hence, the values of equivalent modulus reported by Ganghoffer and Gent[16] are most probably inaccurate. It follows that further quantities derived from Ganghoffer's and Gent's[16] computations, such as energy release rates, are most probably also inaccurate. The improved mesh design, with focused arrangements, is therefore used for all other simulations in the present paper.

Elastic layer confinement

Figure 4 displays the variation of the equivalent modulus as a function of the elastic layer confinement, h/a, ranging from 0.02 to 50. The results are obtained

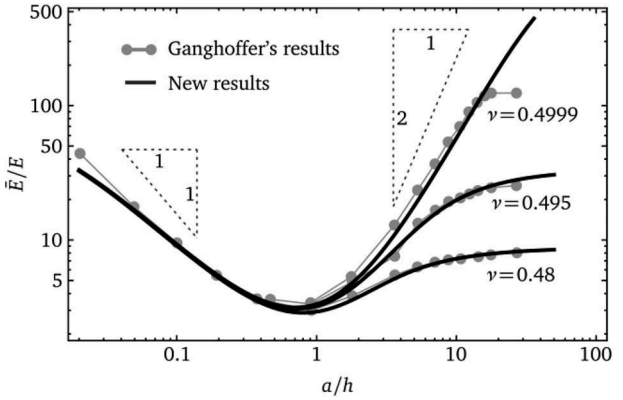

Figure 4. Numerically obtained equivalent modulus in terms of the elastic layer confinement, a/h, for various Poisson's ratios, ν (black lines, designated "New results" in the legend). The radius of the elastic layer was 50 times the punch radius. The gray dots, designated 'Ganghoffer's results' in the legend, represent the Ganghoffer and Gent results reported in ref.[16].

using fine increments of h/a, resulting in smooth curves, and are computed for Poisson's ratios 0.48, 0.495, and 0.4999. The equivalent modulus varies dramatically with confinement, in accordance with the results previously reported by Ganghoffer and Gent[16]. Starting from a very thick, unconfined layer ($h \gg a$), the equivalent modulus decreases monotonically with decreasing layer thickness. In the unconfined limit, the equivalent modulus scales nearly proportionally with a/h for all Poisson's ratios. For specific Poisson's ratios minima occur for the equivalent modulus at values of a/h ranging between 0.68 and 0.84. That is in contrast to a single minimum at $a/h = 1$ for all Poisson's ratios reported in ref.[16]. For greater confinement ($a/h > 0.84$), the equivalent moduli increase again, most likely because lateral retraction of the material is suppressed with that constraint stiffening the response. However, the resulting values of equivalent modulus depend strongly on compressibility (*i.e.* Poisson's ratio), in contrast to the behavior for thick, unconfined layers. As an example, it can be seen that the equivalent modulus for $a/h = 10$ doubles for a slight increase of Poisson's ratio from $\nu = 0.495$ to $\nu = 0.4999$. We note that this increase in Poisson's ratio at fixed Young's modulus involves a 50-fold increase in the bulk modulus, indicating that the associated increase in equivalent modulus occurs largely due to an increased contribution from hydrostatic stress. Interestingly, for very thin, nearly incompressible layers, with $\nu = 0.4999$, the equivalent modulus exhibits scaling that is close to being proportional to $(a/h)^2$. Such scaling may represent the limiting behavior for, thin, wide, confined, incompressible layers[24].

In addition to the results for the equivalent modulus obtained by the improved mesh design, the original values published in ref.[16] are plotted in Figure 4. It can be seen that there is reasonable agreement among our new results and those of Ganghoffer and Gent[16] for $a/h < 10$, although there is a modest discrepancy in the results for the thickest layers. This

agreement continues for very thin layers in the case of a Poisson's ratio of 0.48, and perhaps also for a Poisson's ratio of 0.495, though there appears to be a divergence in the latter case for extremely thin layers with $a/h > 20$. In the case of the least compressible material, with Poisson's ratio 0.4999, it is very clear that there is disagreement for the very thinnest layers. The observed discrepancies in the values of equivalent modulus may originate for the following reasons: (i) Ganghoffer and Gent obtained their results using a coarser mesh as discussed above; (ii) In addition, these authors modeled the punch as a deformable object having an elastic modulus 10^8 times greater than that of the film, whereas in our simulations the punch is rigid; (iii) In our simulations, the layer radius, R, was set to $50a$, whereas in ref.[16] it is reported that R was chosen to be at least three times the radius of the punch, although no exact values are stated.

Effect of the radius of the layer

A comprehensive study of the effect of the radius, R, of the layer on the equivalent modulus has not yet been reported in the literature. However, we find it can have a significant effect on the equivalent modulus. Figure 5 demonstrates the effect of the value of R/a on the equivalent modulus; the equivalent modulus is now shown as a function of h/a for various Poisson's ratios, in contrast to being plotted against a/h as in Figure 4. Two characteristic regimes are identified: (i) For highly confined layers ($h/a \leq 0.02$), the value R/a has no significant effect on the results, but, as noted above, Poisson's ratio has a prominent influence on the equivalent modulus. (ii) For unconfined layers ($h/a \geq 10$), the effect of Poisson's ratio is negligible, as also noted above, but the radius of the layer is found to have a significant influence on the equivalent modulus. As one would expect, the equivalent modulus equals Young's modulus when the layer is the same diameter as the punch, but rises with increasing extent of the layer beyond the perimeter of the punch. This behavior reflects the constraint that material around the contact zone imposes on the deformations that occur near the punch; at the largest radii and thicknesses of the layer, the solution becomes akin to the indentation of a rigid punch into an elastic half-space. These results are further underpinned by Figure A1 and Figure A2 (see Appendix) that show graphs of normalized equivalent moduli versus Poisson's ratio for specific values of h/a and of normalized equivalent moduli versus layer radius for specific values of Poisson's ratio, respectively. Overall, there exists a transition region from $0.02 < h/a < 10$ where both parameters affect the equivalent modulus.

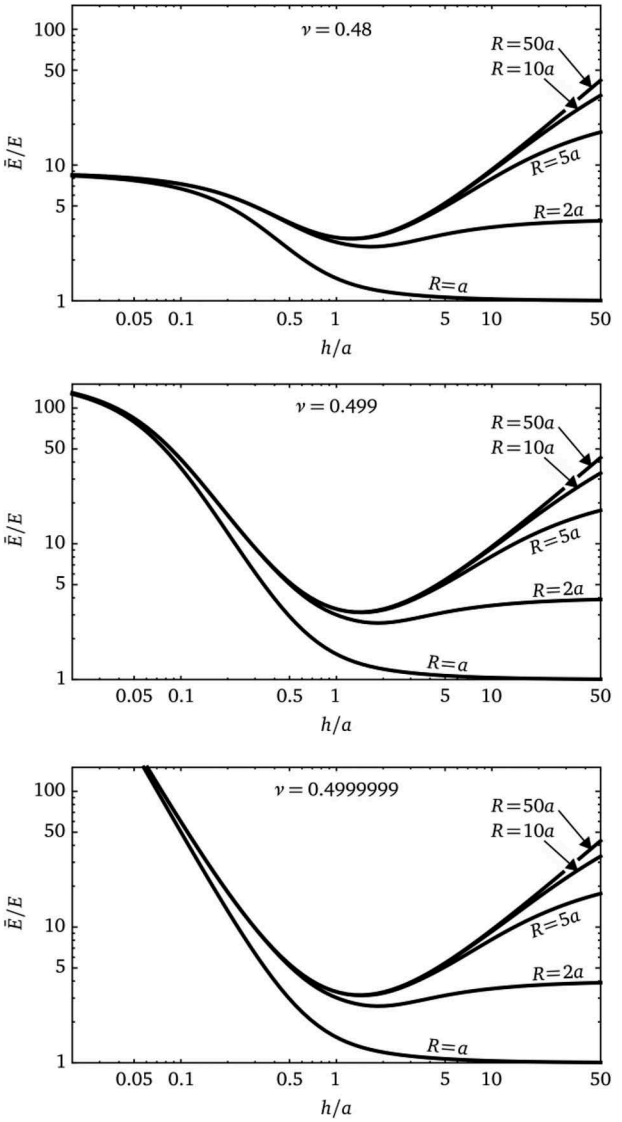

Figure 5. Normalized equivalent modulus as a function of layer thickness normalized by punch radius in terms of the radius, *R*, of the layer for various Poisson's ratios, *v*.

Fitted analytical functions for the equivalent modulus

This section presents an analytical function for the equivalent modulus that we fitted to the numerical results. The function is fitted to the finite element results for $R = 50a$, because these adequately approximate the effect of a layer having infinite radius within the range of confinement ratios, h/a, from 0.02 to 50. Therefore, the function developed is suitable for sheets of elastic material having a radius very much larger than that of the punch. The main goal in this section is to find a suitable function that can be used to represent the equivalent modulus

for all values of Poisson's ratio in the range $0.48 \leq \nu \leq 0.5$. Many candidate functions were investigated. The one chosen has the form:[1]

$$\frac{\bar{E}}{E} = \frac{K_1 + h/a}{K_2 + (h/a)^{K_3}} + \frac{K_4 + h/a}{K_5 + (h/a)^{K_6}}, \tag{5}$$

where the parameters K_i $(i = 1 \ldots 6)$ are functions of Poisson's ratio as follows:

$$\begin{aligned}
K_1 &= 0.1811 - 33.6939(0.5 - \nu)^{0.715} + 5.2574\nu \\
K_2 &= -3.531 + 2.3473(0.5 - \nu)^{0.5256} + 9.2434\nu \\
K_3 &= -30.12 - 0.4099(0.5 - \nu)^{0.2384} + 59.1455\nu \\
K_4 &= 14.5412 + 3.8871(0.5 - \nu)^{0.5213} - 28.0909\nu \\
K_5 &= 2.266 + 199.591(0.5 - \nu)^{1.9625} - 4.5322\nu \\
K_6 &= 21.5731 - 25.3997(0.5 - \nu)^{0.7325} - 39.1534\nu
\end{aligned} \tag{6}$$

Consequently, by combining Equations. (5) and (6) we arrive at the function $\bar{E}/E = \hat{E} = \hat{E}(h/a, \nu)$ that can be used to determine the equivalent modulus in the ranges $h/a = 0.02$ to 50 and $\nu = 0.48$ to 0.5. The accuracy of this function is demonstrated in Figure 6, where it is compared with the finite element results. One can see that the selected function provides an accurate approximation for the equivalent modulus in the entire domain under investigation.

For $\nu = 0.499999$ and $h/a < 0.1$, the equivalent modulus scales with $(h/a)^{-2}$, which represents the severely confined limit for incompressible elastic films. In Equation. (5) the relevant asymptotic behavior is captured by the 2nd term on the right hand side, which, when $\nu = 0.5$, approaches very close to $(K_4 + h/a)(a/h)^2$ while the 1st term is negligible for small h. In contrast, in the unconfined limit $(h/a > 10)$, the equivalent modulus scales linearly with h/a for $R = 50a$, but is insensitive to the Poisson's ratio.

Energy release rate

Based on the analytical function for the equivalent modulus, Equations. (5) and (6), the energy release rate can be derived to characterize adhesion. The equivalent modulus can be inserted into Equation. (1) to determine G as follow:

[1]In our approach to finding a suitable function, we tried over 500 possibilities. Our preference was to find the simplest possible function, such as sums of ratios of polynomials as in Equation. (5). Our choice of the specific form given in Equation. (5) was favored by the fact that, when we plotted each K_i versus Poisson's ratio, we found that the resulting graphs could be accurately characterized by polynomials. We computed R-squared coefficients and found all to be ≥ 0.99. We found it preferable to use $(0.5 - \nu)$ as the argument in the nonlinear term in the polynomials due to our focus on materials that are almost incompressible.

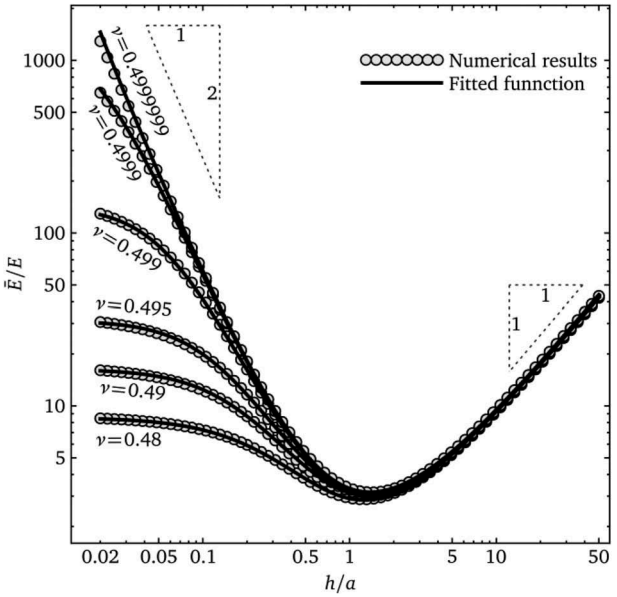

Figure 6. Comparison of the fitted analytical function (solid lines) with finite element results (circles) for the equivalent modulus for various Poisson's ratios.

$$G = \frac{\partial U}{\partial A} = \frac{\partial}{\partial A}\left(\bar{E} \times \frac{u^2 a^2 \pi}{2h}\right) = \frac{\partial}{\partial a}\left(\bar{E} \times \frac{u^2 a^2 \pi}{2h}\right)\frac{1}{2a\pi}$$
$$= \frac{u^2}{2h}\left(\frac{\partial \bar{E}}{\partial a} \times \frac{a}{2} + \bar{E}\right) \tag{7}$$

We introduce $h/a = \eta$ for simplicity. Then

$$\frac{\partial \bar{E}}{\partial a} = \frac{\partial \bar{E}}{\partial \eta}\frac{\partial \eta}{\partial a} = -\frac{h}{a^2}\frac{\partial \bar{E}}{\partial \eta} \tag{8}$$

Therefore, the energy release rate can be written as

$$G = \frac{u^2}{4h}\left(2\bar{E} - \eta\frac{\partial \bar{E}}{\partial \eta}\right) \tag{9}$$

A dimensionless normalized energy release rate is defined as:

$$\bar{G} = \frac{Gh}{u^2 E} = \left(\frac{\bar{E}}{2E} - \frac{\eta}{4E}\frac{\partial \bar{E}}{\partial \eta}\right) \tag{10}$$

Figure 7 shows results for the normalized energy release rate, $\bar{G}$, as functions of h/a for specific Poisson's ratios. For thick, unconfined layers, $\bar{G}$ is insensitive to the material's Poisson's ratio, whereas for thin, confined layers, the normalized energy release rate differs by up to two orders of magnitude depending on Poisson's ratio. Figure 7 exhibits minima for $\bar{G}$ at confinement

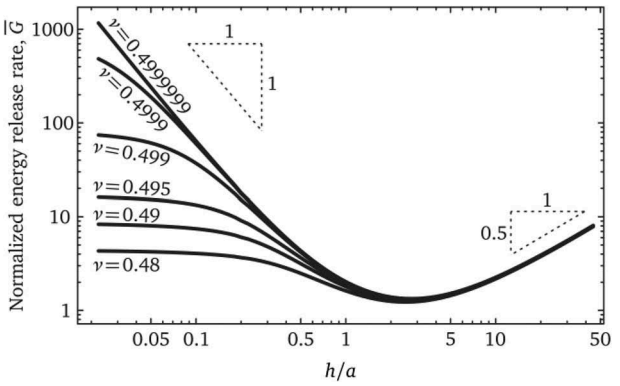

Figure 7. Normalized energy release rate as a function of h/a for different Poisson's ratios.

Table 2. Critical values for h/a and a/h, defined to be where the normalized energy release rate, $\bar{G}$, is a minimum (see Figures 7 and 8), and the associated minimum value of $\bar{G}$. The values denoted by [(a)] are those given by Webber et al.[2].

Poisson's ratio	h/a where $\bar{G}$ has a minimum, *i.e.* η^*	a/h where $\bar{G}$ has a minimum, *i.e.* $(\eta^*)^{-1}$	Associated minimum value of $\bar{G}$
0.48	2.0935	0.4777	1.2869
0.49	2.2729	0.4399	1.3710
0.5	2.2804	0.4385	1.4204
0.5[(a)]	2.201[(a)]	0.45[(a)]	1.267[(a)]

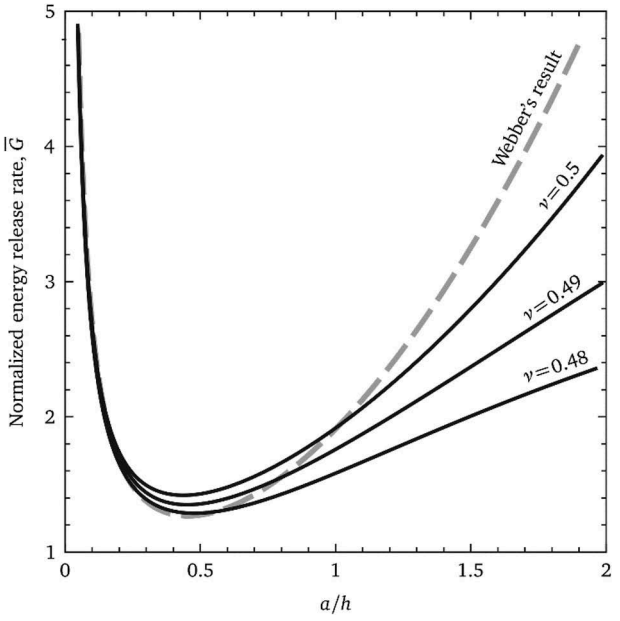

Figure 8. Comparison of the new results for the normalized energy release rate with the results reported in Webber et al.[2].

ratios summarized in Table 2, where those minimum values for $\bar{G}$ are also given. These critical confinements, η^* or $(\eta^*)^{-1}$, correspond to distinct detachment mechanisms of stable and unstable growth of the detached area, as previously reported by Webber et al.[2]. Detachment commences when the energy release rate equals the adhesion energy, w. Figure 8 show that $dG/da < 0$ for $a/h < (\eta^*)^{-1}$ (see Table 2). Hence, if $a/h < (\eta^*)^{-1}$ complete detachment occurs immediately upon G becoming equal to w as the imposed punch displacement is increased. This occurs because G increases with decreasing contact radius, a, resulting in an unstable growth of the detached area of the punch. In contrast, $dG/da > 0$ for $a/h > (\eta^*)^{-1}$. In this situation as the imposed displacement of the punch is increased, detachment starts when G becomes equal to w, as before. However, G decreases with decreasing contact radius, and thus the imposed displacement on the punch must be increased if further increments of detachment are to occur. This process must be continued until the critical confinement, $a/h = (\eta^*)^{-1}$, is achieved, at which stage the advancing detachment shifts from stable to unstable growth.

In Figure 8, the results obtained from Equations. (5), (6), and (10) based on our new finite element calculations are compared with the equivalent result from Webber et al. [2], where their result is given for a Poisson's ratio of 0.5, *i.e.* an incompressible material. Our critical values of a/h for all Poisson's ratios are in reasonable agreement with those of Webber et al.[2], and our critical values do not vary very significantly with Poisson's ratio (see Table 2). However, the results from Webber et al.[2] underestimate the minimum value of $\bar{G}$ by about 10% for a Poisson's ration of 0.5 (see Table 2), and overestimates $\bar{G}$ significantly for thin, confined layers having $a/h > 1.1$ for all Poisson's ratios. It is most likely that this discrepancy originates from the relatively inaccurate finite element results published by Ganghoffer and Gent[16], that served as a basis for the analytical function for the energy release rate deduced in the work of Webber et al.[2].

Interfacial stress distribution

To document the stress at the interface between the rigid punch and the elastic layer, we provide the plots in Figure 9, which are all obtained for the elastic layer having a radius of $50a$. We note that the dominant interfacial stress component is typically σ_z, *i.e.* the normal traction on the contact, so we have restricted attention to that component. Figure 9 shows the normalized stress $\sigma_z/\bar{\sigma}$ at the interface for three values of Poisson's ratio, where $\bar{\sigma} = \bar{E}\bar{\varepsilon} = \bar{E}h/u$ is the average stress at the interface. The stress is shown as a function of both the confinement ratio, h/a, and ξ/a, where ξ is the distance from the corner (location D) toward the center of the punch along the interface. Since we have

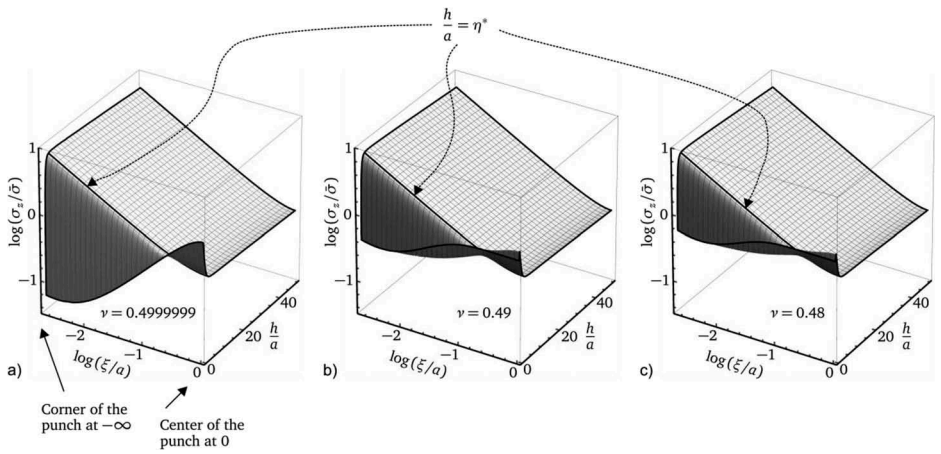

Figure 9. Normal stress, $\sigma_z/\bar{\sigma}$, along the interface (logarithmic scales base 10) between the rigid punch and the elastic layer as a function of layer confinement h/a for Poisson's ratio (**a)** 0.4999999, (**b)** 0.49, and (**c)** 0.48. The coordinate ξ corresponds to the distance from the perimeter toward the center of the punch (see Figure 1). The solid line, labeled with η^*, highlights the stress distribution at the critical confinement ratio $h/a = \eta^*$ (see Table 2).

stress singularities at the corner D (see Figure 1) the interfacial stress is plotted on a logarithmic scale (base 10)[25,26]. The critical confinement value, denoted as η^*, at which the normalized energy release rate exhibits a minimum, is emphasized by use a black line along the plot at that location. The following observations can be made:

(i) There is a distinct corner stress singularity for $h/a > \eta^*$, exhibited by the high values of stress near the corner D in this case. The strength of the stress singularity (represented by the linear slope of the stress distribution close to the corner) and its magnitude for a given Poisson's ratio are similar for all confinements h/a larger than η^*. Hence, for thick, unconfined layers, the separation most probably occurs via edge crack detachment. Upon crack initiation, the energy release rate further increases with decreasing contact area (see Figures 7 and 8), resulting in an unstable crack growth, as observed in several reports[23,25].

(ii) There is a transition region for h/a just below η^*, where the strength and magnitude of the stress singularity decreases while, simultaneously, the stress at the center of contact increases. The propensity for edge crack detachment remains; however, in contrast to unconfined layers, the energy release rate decreases during detachment leading to stable crack growth, whereby instabilities of the crack front have often been observed[19–21].

(iii) For highly confined layers with h/a much smaller than η^*, the stress near the center of the contact is high and falls significantly as the

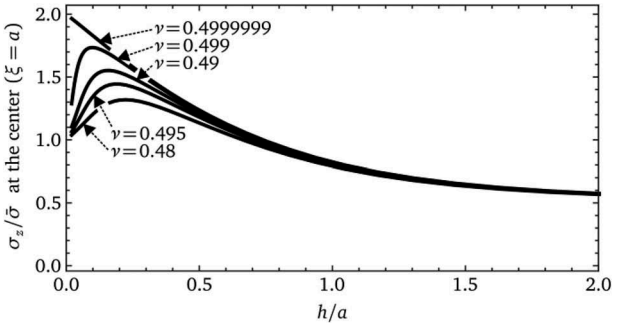

Figure 10. Normal stress, $\sigma_z/\bar{\sigma}$, on the interface between the rigid punch and the elastic layer at the center of the punch as a function of the layer confinement, h/a, for various Poisson's ratios.

corner D is approached. Note that the stress singularity at the corner, though it is present, is not dominant. In the case where the elastic layer has properties that most closely approach incompressible elasticity (ν = 0.4999999) and is subject to the greatest degree of confinement ($h/a = 0.02$), the normalized stress at the center of the punch reaches a value of about 2 in accordance with previous estimates based on incompressibility of the elastic layer[22,27]. However, for layers that are more compressible ($\nu < 0.4999999$), the maximum stress at the center of the punch remains below 2. In Figure 10, the stress at the center of the punch is shown for specific values of Poisson's ratio as a function of h/a. It can be seen that this stress rises with each Poisson's ratio as the degree of confinement becomes more severe, *i.e.* as h/a diminishes. However, at a specific value of the Poisson's ratio, there is a maximum in each plot, and the stress at the center of the punch then falls as h/a is increased. It can be seen in Figure 10 that this maximum value increases with Poisson's ratio, and occurs at more severe degrees of confinement as that ratio gets larger. Due to the reduced magnitude of the corner stress singularity, the propensity for edge crack detachment decreased. Now, the interfacial detachment most likely occurs via cavitation and fibrillation or the propagation of penny-shaped cracks depending on the confinement, the film elasticity and the Poisson's ratio[28]. As in ii), the energy release rate decreases during progressive detachment, resulting in stable crack growth[2,28,29].

It should be noted that our description of the distinct detachment mechanisms, though qualitative, is in line with earlier reports[2,28,29]. A detailed analysis regarding which mechanism is active, dependent on the interfacial stress distribution and the energy release rate, will be undertaken in future research.

Discussion

The elastic deformation and adhesion associated with a rigid punch attached to an elastic layer that, in turn, is immobilized to a rigid substrate, has been investigated numerically. The finite element model used in the present study was chosen carefully to ensure accuracy based on comparison of different mesh designs. As a result, a mesh design that includes refinement at the corner of the punch and at the corner of the elastic layer near the substrate, capturing expected stress singularities, was identified to deliver the most accurate results. With that choice of mesh, the problem of a rigid punch attached to and deforming an elastic layer was solved for various values of Poisson's ratio close to 0.5. The punch was displaced normally to the surface of the elastic layer, causing an axial strain in the elastic layer between the punch and the rigid substrate. The average stress applied axially to the punch was computed, and an equivalent modulus of the system was obtained by dividing the average stress on the punch by the axial strain in the elastic layer. This equivalent modulus was obtained as a function of layer confinement, defined as the ratio of the thickness of the layer to the radius of the punch, of the layer's Poisson's ratio, and, for the first time, of the radius of the elastic layer. Starting from unconfined layers, the equivalent modulus monotically decreased with increasing confinement. Here, the equivalent modulus is found to be insensitive to the Poisson's ratio, but significantly varies with the radius of the layer. Higher radii of the layer lead to higher equivalent moduli, most probably due to the higher amount of material around the contact involved in the elastic deformation. For values of a/h between 0.68 and 0.84, minima for the equivalent modulus were obtained for different Poisson's ratios. For greater confinement, the equivalent moduli increased again. Now the increase significantly varies with the Poisson's ratio, but is insensitive to the extent of the layer. The stiffening of highly confined layers is most likely caused by the suppression of lateral material retraction that strongly varies with the material's compressibility (*i.e.* Poisson's ratio). Within the range of parameters investigated, the numerical results were fitted by a two-parameter analytical function that, in turn, was used to calculate the energy release rate as a measure for the adhesion of films. For highly confined layers, the energy release rate significantly varies with Poisson's ratio. Hence, the material's compressibility is identified as a critical parameter for adhesion performance.

In experiments, incompressible materials (*i.e.* $\nu = 0.5$) are often assumed, but slight deviations cannot be ruled out, that consequently may lead to overestimates of adhesion energies. In such materials that are nearly, but not quite, incompressible, nucleation of small interfacial

cavities is likely to result in smaller "effective" adhesion energies at the macroscopic scale. Plots of normalized energy release rate versus the diameter of the adhered surface obtained from our results typically show a minimum that separates regimes of stable and unstable crack growth. These results can be further correlated with interfacial stress distributions, that, most likely, provide qualitative explanations for distinctions in mechanisms, such as self-similar contraction of the adhered area, cavitation and fingering, by which a stiff punch detaches from an elastic layer, as observed in several experiments[1–3,18,23,29].

Conclusions

Numerical analysis was performed to determine the equivalent modulus of an isotropic elastic layer confined by stiff adjacent materials. For the equivalent modulus we developed an analytical function from our numerical results dependent on material and geometric parameters. This function has been utilized to deduce the energy release rate for detachment of a punch from the confined layer in terms of material and geometric parameters. The following conclusions can be drawn:

- A mesh design that includes refinement at locations where stress singularities are expected provides the most accurate results for the equivalent modulus.
- The equivalent modulus of a highly confined layer (*i.e.* with thickness to radius ratio $h/a \leq 0.02$) depends on its Poisson's ratio. In contrast, the influence of the material's compressibility (*i.e.* Poisson's ratio) is negligible for unconfined (*i.e.* thick) layers.
- The equivalent modulus for unconfined layers ($h/a \geq 10$) depends on the radius of the elastic film, whereas the extent of the layer does not affect the stiffness of very thin films.
- In a tack test experiment, edge crack detachment, fingering instabilities and the detachment via cavitation or penny-shaped cracks are common mechanisms. Which of them is active depends on the extent of layer confinement that determines the interfacial stress distribution and the rate of change of the energy release rate during detachment propagation.

Funding

RH acknowledges partial funding from the European Research Council under the European Union's Seventh Framework Programme (FP/2007-2013)/ERC Advanced Grant

"Switch2Stick" Agreement no. 340929 and by the German Research Foundation (Deutsche Forschungsgemeinschaft) through grant No. HE 7498/1-1.

ORCID

René Hensel http://orcid.org/0000-0002-9623-2118

References

[1] Shull, K. R.; Ahn, D.; Chen, W.-L.; Flanigan, C. M.; Crosby, A. J. *Macromol. Chem. Phys*. 1998, *199*, 489–511. DOI: 10.1002/(ISSN)1521-3935.
[2] Webber, R. E.; Shull, K. R.; Roos, A.; Creton, C. *Phys. Rev. E*. 2003, *68*, 021805. DOI: 10.1103/PhysRevE.68.021805.
[3] Bartlett, M. D.; Crosby, A. J. *Langmuir*. 2013, *29*, 11022–11027. DOI: 10.1021/la4013526.
[4] Fischer, S. C. L.; Kruttwig, K.; Bandmann, V.; Hensel, R.; Arzt, E. *Macromol. Mater. Eng*. 2017, *302*, 1600526. DOI: 10.1002/mame.v302.5.
[5] Roos, A.; Creton, C.; Novikov, M. B.; Feldstein, M. M. *J. Polym. Sci. Part B Polym. Phys*. 2002, *40*, 2395–2409. DOI: 10.1002/(ISSN)1099-0488.
[6] Peak, C. W.; Wilker, J. J.; Schmidt, G. *Colloid Polym. Sci*. 2013, *291*, 2031–2047. DOI: 10.1007/s00396-013-3021-y.
[7] Yuk, H.; Zhang, T.; Lin, S.; Parada, G. A.; Zhao, X. T. *Nat. Mater*. 2015, *15*, 190–196. DOI: 10.1038/nmat4463.
[8] Bacca, M.; Booth, J. A.; Turner, K. L.; McMeeking, R. M. *J. Mech. Phys. Solids*. 2016, *96*, 428–444. DOI: 10.1016/j.jmps.2016.04.008.
[9] Kim, S.; Sitti, M.; Hui, C.-Y.; Long, R.; Jagota, A. *Appl. Phys. Lett*. 2007, *91*, 161905. DOI: 10.1063/1.2801371.
[10] Brady, R. F.; Singer, I. L. *Biofouling*. 2000, *15*, 73–81. DOI: 10.1080/08927010009386299.
[11] Chung, J. Y.; Chaudhury, M. K. *J. Adhes*. 2005, *81*, 1119–1145. DOI: 10.1080/00218460500310887.
[12] Hui, C.-Y.; Long, R.; Wahl, K. J.; Everett, R. K. *J. R. Soc. Interface*. 2011, *8*, 868–879. DOI: 10.1098/rsif.2010.0567.
[13] Kendall, K.;. *J. Phys. D. Appl. Phys*. 1971, *4*, 1186–1195. DOI: 10.1088/0022-3727/4/8/320.
[14] Barquins, M.; Maugis, D. *J. Adhes*. 1981, *13*, 53–65. DOI: 10.1080/00218468108073174.
[15] Maugis, D.; Barquins, M. *J. Phys. D. Appl. Phys*. 1983, *16*, 1843–1874. DOI: 10.1088/0022-3727/16/10/010.
[16] Ganghoffer, J. F.; Gent, N. *J. Adhes*. 1995, *48*, 75–84. DOI: 10.1080/00218469508028155.
[17] Griffith, A. A.;. *Philos. Trans. R. Soc. A Math. Phys. Eng. Sci*. 1921, *221*, 163–198. DOI: 10.1098/rsta.1921.0006.
[18] Shull, K. R.;. *Mater. Sci. Eng. R Rep*. 2002, *36*, 1–45. DOI: 10.1016/S0927-796X(01)00039-0.
[19] Ghatak, A.; Chaudhury, M. K.; Shenoy, V.; Sharma, A. *Phys. Rev. Lett*. 2000, *85*, 4329–4332. DOI: 10.1103/PhysRevLett.85.4329.
[20] Ghatak, A.; Chaudhury, M. K. *Langmuir*. 2003, *19*, 2621–2631. DOI: 10.1021/la026932t.

[21] Shull, K.; Flanigan, C.; Crosby, A. *Phys. Rev. Lett*. 2000, *84*, 3057–3060. DOI: 10.1103/PhysRevLett.84.3057.
[22] Balijepalli, R. G.; Fischer, S. C. L.; Hensel, R.; McMeeking, R. M.; Arzt, E. *J. Mech. Phys. Solids*. 2017, *99*, 357–378. DOI: 10.1016/j.jmps.2016.11.017.
[23] Fischer, S. C. L.; Arzt, E.; Hensel, R. *ACS Appl. Mater. Interfaces*. 2017, *9*, 1036–1044. DOI: 10.1021/acsami.6b11642.
[24] Doi, M.; Yamaguchi, T. *J. Nonnewton. Fluid Mech*. 2007, *145*, 52–56. DOI: 10.1016/j.jnnfm.2006.12.006.
[25] Khaderi, S. N.; Fleck, N. A.; Arzt, E.; McMeeking, R. M. *J. Mech. Phys. Solids*. 2015, *75*, 159–183. DOI: 10.1016/j.jmps.2014.11.004.
[26] Balijepalli, R. G.; Begley, M. R.; Fleck, N. A.; McMeeking, R. M.; Arzt, E. *Int. J. Solids Struct*. 2016, *85*, 160–171. DOI: 10.1016/j.ijsolstr.2016.02.018.
[27] Lindsey, G. H.;. Triaxial Fracture Studies. *J. Appl. Phys*. 1967, *38*, 4843–4852. DOI: 10.1063/1.1709232.
[28] Creton, C.; Lakrout, H. *J. Polym. Sci. Part B Polym. Phys*. 2000, *38*, 965–979. DOI: 10.1002/(ISSN)1099-0488.
[29] Crosby, A. J.; Shull, K. R.; Lakrout, H.; Creton, C. *J. Appl. Phys*. 2000, *88*, 2956–2966. DOI: 10.1063/1.1288017.

Appendix

The equivalent modulus is insensitive to Poisson's ratio for unconfined thick layers ($h/a \geq 10$), but that ratio becomes an important parameter with increasing confinement (Figure A1). As an example, the increase of Poisson's ratio from 0.48 to 0.4999999 results in an increase of the equivalent modulus by about two orders of magnitude as shown in Figure A1f. In contrast, the equivalent modulus is insensitive to the radius of the elastic layer for highly confined thin layers ($h/a \leq 0.02$), but is influenced by that radius with decreasing confinement (Figure A2). As an example, an increase of the aspect ratio, R/a, of the layer from 1 to 10 leads to an increase of the equivalent modulus by about one order of magnitude as shown in Figure A2d.

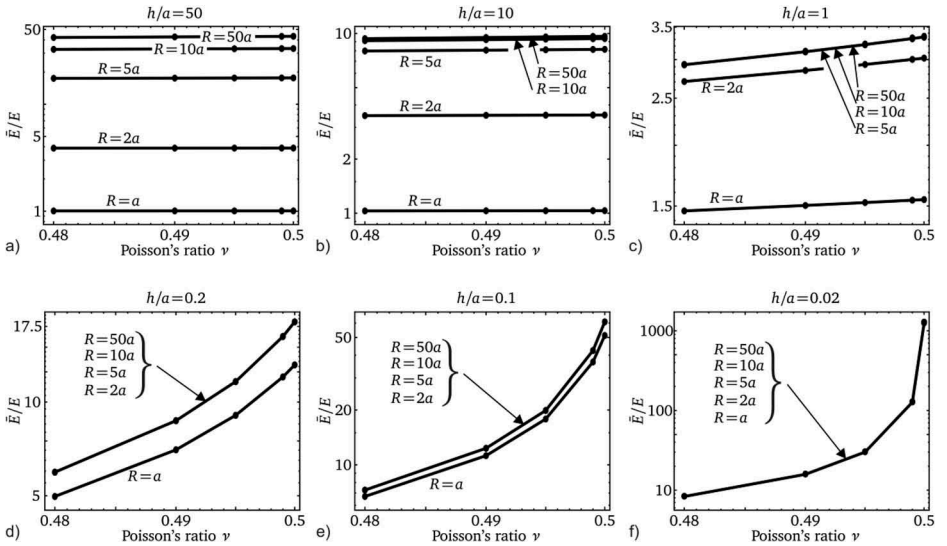

Figure A1. Normalized equivalent modulus as a function of Poisson's ratio for various radii of the elastic layer and various confinement ratios: **(a)** $h/a = 50$, **(b)** $h/a = 10$, **(c)** $h/a = 1$, **(d)** $h/a = 0.2$, **(e)** $h/a = 0.1$, and **(f)** $h/a = 0.02$.

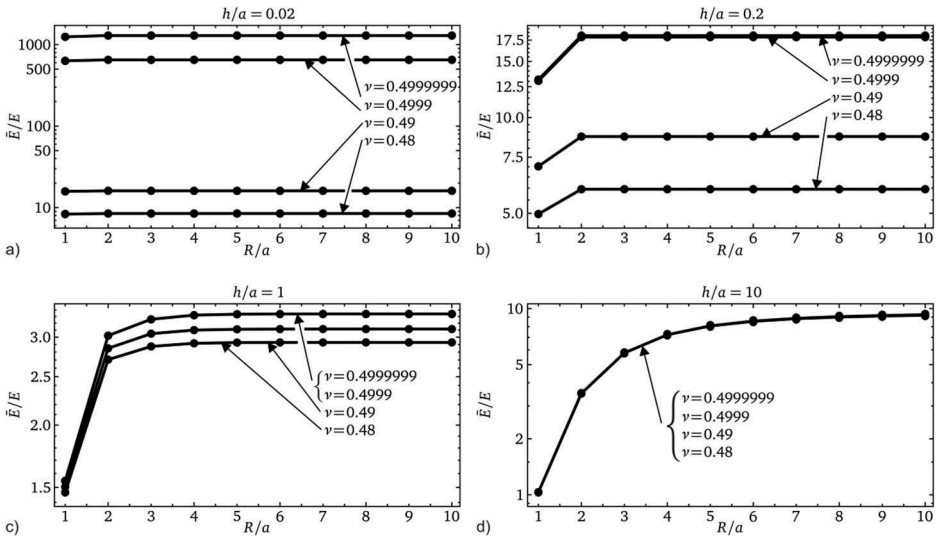

Figure A2. Normalized equivalent modulus as a function of the radius of the elastic layer normalized by the punch radius, R/a, for various Poisson's ratios and confinement ratios: **(a)** $h/a = 0.02$, **(b)** $h/a = 0.2$, **(c)** $h/a = 1$, and **(d)** $h/a = 10$.